Article No. mb981913 *J. Mol. Biol.* (1998) **280**, 687–701

JMB

The NMR Solution Structure of Human Glutaredoxin in the Fully Reduced Form

Chaohong Sun, Marcelo J. Berardi and John H. Bushweller*

Department of Chemistry
Dartmouth College, Hanover
NH 03755, USA

The determination of the nuclear magnetic resonance (NMR) solution structure of fully reduced human glutaredoxin is described. A total of 1159 useful nuclear Overhauser effect (NOE) upper distance constraints and 187 dihedral angle constraints were obtained as the input for the structure calculations for which the torsion angle dynamics program DYANA has been utilized followed by energy minimization in water with the AMBER force field as implemented in the program OPAL. The resulting 20 conformers have an average root-mean-square deviation value relative to the mean coordinates of 0.54 Å for all the backbone atoms N, C^{α} and C′, and of 1.01 Å for all heavy atoms. Human glutaredoxin consists of a four-stranded mixed β-sheet composed of residues 15 to 19, 43 to 47, 72 to 75 and 78 to 81, and five α-helices composed of residues 4 to 9, 24 to 34, 54 to 65, 83 to 91, and 94 to 100. Comparisons with the structures of *Escherichia coli* glutaredoxin-1, pig liver glutaredoxin and human thioredoxin were made. Electrostatic calculations on the human glutaredoxin structure and that of related proteins provide an understanding of the variation of pK_a values for the nucleophilic cysteine in the active site observed among these proteins. In addition, the high-resolution NMR solution structure of human glutaredoxin has been used to model the binding site for glutathione and for ribonucleotide reductase B1 by molecular dynamics simulations.

Keywords: glutaredoxin; glutathione; nuclear magnetic resonance; protein structure determination; ribonucleotide reductase

**Corresponding author*

Introduction

Glutaredoxins are a family of proteins involved in electron transfer reactions *via* the reversible oxidation of two active-site thiols to a disulfide bond. Glutaredoxins have now been identified in numerous species including *Escherichia coli*, bacteriophage T4, vaccinia virus, yeast, rabbit, pig, and human (Ahn & Moss, 1992; Gan & Wells, 1987a; Gan *et al*., 1990; Höög *et al*., 1983; Hopper *et al*., 1989; Johnson *et al*., 1991; Klintrot *et al*., 1984; Minakuchi *et al*., 1994; Padilla *et al*., 1995). This important family of protein disulfide reductants has been shown to play numerous important roles in the cell. They are essential for the glutathione-dependent reduction of ribonucleotides by ribonucleotide reductase (Holmgren, 1976, 1979; Luthman *et al*., 1979; Luthman & Holmgren, 1982). They have also been shown to play a role in the reduction of sulfate (Russel *et al*., 1990; Tsang, 1981), arsenate (Gladysheva *et al*., 1994; Wells *et al*., 1990), and ascorbate (Ahn & Moss, 1992; Gravina & Mieyal, 1993). They preferentially reduce glutathione-containing mixed disulfides (Gravina & Mieyal, 1993; Jung & Thomsa, 1996) due to the glutathione binding site present on the protein (Bushweller *et al*., 1994) . This preference for GSH-containing mixed disulfides also means that these proteins will play a key role in the glutathionylation and deglutathionylation of proteins which is an important element of the cellular response to oxidative stress. Glutaredoxins have also been shown to accelerate the

Abbreviations used: *E. coli* Grx-1, *E. coli* glutaredoxin-1; Grx, glutaredoxin; huTrx, human thioredoxin; GR, glutathione reductase; GSH, glutathione; GSSG, oxidized glutathione; NDP, diphosphate ribonucleotide; dNTP, diphosphate deoxyribonucleotide; NMR, nuclear magnetic resonance; NOE, nuclear Overhauser effect; NOESY, nuclear Overhauser effect spectroscopy; RR, reduced ribonucleotide reductase; T_2, transverse relaxation time; Trx, thioredoxin; RMSD, root-mean-square-deviation; 3D, three-dimensional; MD, molecular dynamics; ppm, parts per million.

E-mail address of the corresponding author: john.h.bushweller@dartmouth.edu

0022–2836/98/290687–15 $30.00/0

in vitro rate of PDI-mediated folding of proteins (Lundstrom-Ljung & Holmgren, 1995). Very recently, human glutaredoxin has been shown to regulate the activity of HIV-1 protease and to be packaged into HIV viral particles (Davis *et al*., 1997). Interestingly, vaccinia virus also packages its virally encoded glutaredoxin into its viral particles (Ahn & Moss, 1992), suggesting a possible functional role for glutaredoxins in viral pathogenesis.

Glutaredoxins are part of a structural superfamily of proteins which also includes thioredoxin, DsbA, GSH-transferase, and GSH-peroxidase, all of which share a common fold. Glutaredoxins are functionally distinguished from the related disulfide reductants termed thioredoxins by their differential reactivity. Glutaredoxins are reduced by GSH (see Figure 1) but not by thioredoxin reductase, whereas thioredoxins are reduced by the corresponding thioredoxin reductase but not by GSH. As mentioned above, glutaredoxins preferentially catalyze GSH mixed disulfide oxidoreduction reactions whereas thioredoxin acts as a quite general protein disulfide reductant. In *E. coli*, both thioredoxin and glutaredoxin can function as an effective protein disulfide reductant for ribonucleotide reductase; however, mutants deficient in Grx (Kren *et al*., 1988) and the tenfold lower K_m value of Grx for ribonucleotide reductase (Holmgren, 1979) suggest that Grx may be the dominant *in vivo* reductant. Three-dimensional structures of a number of glutaredoxins have recently been determined including for the oxidized, reduced, and GSH mixed disulfide forms of *E. coli* glutaredoxin-1 (Sodano *et al*., 1991; Xia *et al*., 1992; Bushweller *et al*., 1994), for the oxidized and reduced forms of bacteriophage T4 glutaredoxins (Eklund *et al*., 1992; Ingelman *et al*., 1995), and for oxidized pig liver glutaredoxin (Katti *et al*., 1995).

Glutaredoxins show a high degree of homology in the vicinity of the active site; however, the homology between *E. coli* glutaredoxin–1 in particular and the mammalian glutaredoxin breaks down outside these regions. Human glutaredoxin is longer than its *E. coli* counterpart and is a basic protein, unlike the *E. coli* enzyme, thus it is of significant interest to structurally characterize human glutaredoxin. All the mammalian glutaredoxins studied thus far have two or more cysteine residues in addition to those observed in the active site. Human glutaredoxin possesses three additional cysteine residues (Cys8, Cys79 and Cys83). These additional cysteine residues have been proposed to play a regulatory role because their oxidation leads to inactivation in the case of calf thymus glutaredoxin (Klintrot *et al*., 19984).The presence of this potential site for redox regulation provides an opportunity to examine the potential structural basis for such regulation in this system. Herein we report the high resolution NMR solution structure of the fully reduced form of human glutaredoxin as well as detailed analysis of the implications of the structure on the cysteine pK_a values, binding of GSH, and binding of ribonucleotide reductase.

Results

Collection of conformational constraints and calculation of the three-dimensional structure

A total of 3779 cross-peaks were assigned and integrated in the 60 ms 3D ^{15}N and ^{13}C-edited NOESY spectra of human glutaredoxin. After preprocessing with DYANA to exclude redundant upper distance constraints and to include pseudoatom corrections, a total of 1159 meaningful NOE upper distance constraints were obtained (398 intraresidual, 250 sequential, 220 medium-range, and 283 long-range) corresponding to an average of 11 distance constraints per residue. The distribution of NOE upper distance constraints *versus* the sequence is shown in Figure 2 and ranges from a low of one constraint for Asn52 to a high of 41 constraints for Ile19. A total of 96 $^3J_{HNH\alpha}$ coupling constants for 91 residues (including five Gly) and 91 $^3J_{H\alpha H\beta}$ coupling constants were measured. $^3J_{HNH\alpha}$ coupling constants were obtained from either inverse Fourier transformation of in-phase multiplets from a 2D [^{15}N,^1H] HSQC spectrum (Szyperski *et al*., 1992) or 3D HNHA (Kuboniwa *et al*., 1994) for Gly residues. $^3J_{H\alpha H\beta}$ coupling constants were obtained for 55 residues from analysis of a 3D HACAHB-COSY spectrum (Grzesiek *et al*., 1995). Additionally, qualitative values of $^3J_{NH\beta}$ were obtained from a 3D HNHB spectrum (Archer *et al*., 1991). Analysis with the programs HABAS (Güntert *et al*., 1989) and GLOMSA (Güntert *et al*., 1991) yielded stereospecific assignments for 44 pairs of CH_2 groups including five of the Gly residues and for eight pairs of isopropyl methyl groups of Val and Leu. In addition, stereospecific assignments for 13 of the 15 side-chain amide proton pairs of Asn and Gln were obtained on the

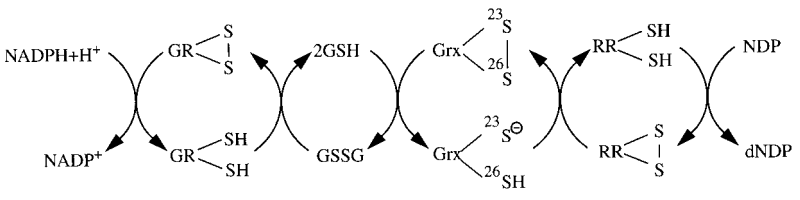

Figure 1. Schematic of ribonucleotide reduction *via* the glutaredoxin system. The active site thiols of glutaredoxin are labeled with the appropriate residue numbers. Nomenclature is as follows: GR-S_2, oxidized glutathione reductase; GR-$(SH)_2$, reduced glutathione reductase; GSH, reduced glutathione; GSSG, oxidized glutathione; Grx-S_2 oxidized Grx; Grx-$(SH)_2$, reduced Grx; NDP, diphosphate ribonucleotide; dNDP, diphosphate deoxyribonucleotide; RR-$(SH)_2$, reduced ribonucleotide reductase; RR-S_2, oxidized ribonucleotide reductase.

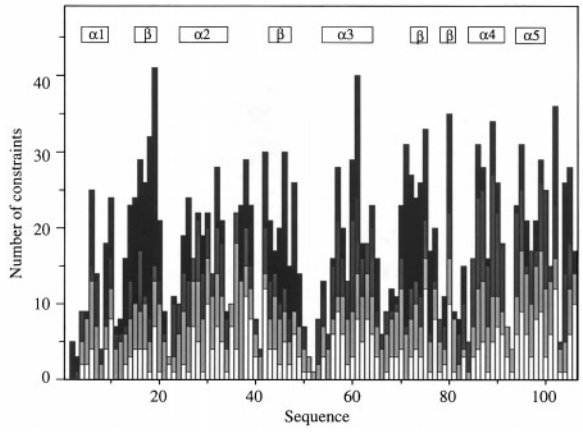

Figure 2. Plot of the number of NOE upper distance constraints in reduced human glutaredoxin *versus* the sequence of the protein. Upper distance limits are classified according to their range: open bars indicate intra-residual constraints, light gray bars indicate sequential constraints, gray bars indicate medium-range constraints, and black bars indicate long-range constraints.

basis of the intensities of intra-residual NOEs between the two amide protons and the β- or γCH2 groups. A total of 65 stereospecific assignments were obtained. The 20 conformers with the lowest residual target function values from DYANA were subjected to energy minimization in a water shell of 6 Å thickness. The 20 final energy-minimized conformers used to represent the solution structure of fully reduced human glutaredoxin have small residual violations of the NOE upper distance constraints and the dihedral angle constraints, as well as low overall energies (Table 1). The coordinates for the 20 conformers have been deposited in the Protein Data Bank with entry number 1JHB.

The NMR solution structure of reduced human glutaredoxin

Figures 3 and 4 show a schematic representation of the fold of the solution structure of human glutaredoxin and a superposition of the 20 conformers obtained after energy minimization, respectively. The global fold of reduced human glutaredoxin is very well-defined as indicated by the average of the pairwise RMSD values for the 20 final conformers relative to their mean coordinates which is 0.54 Å for the entire backbone and 0.41 Å for the secondary structure elements (Table 2). The corresponding value for all heavy atoms relative to their mean coordinates is 1.01 Å (Table 2). An additional indication of the quality of the structure determination can be obtained from an analysis of the conformers with the program PROCHECK (Laskowski *et al*., 1996), which shows 87.6% of the residues to be located in the most-favored region of the Ramachandran plot, 10.7% in additionally allowed regions, 2.0% in generously allowed regions, and only 0.6% in disallowed regions of the Ramachandran plot.

As seen in Figure 3, human glutaredoxin is an α/β protein as are all the other glutaredoxins for which structural information is available (Sodano *et al*., 1991; Xia *et al*., 1992; Bushweller *et al*., 1994; Eklund *et al*., 1992; Ingelman *et al*., 1995; Katti *et al*., 1995). The molecular architecture of human glutaredoxin consists of a four-stranded mixed β-sheet very similar to that observed in *E. coli* glutaredoxin-1 (Sodano *et al*., 1991) composed of residues 15 to 19, 43 to 47, 72 to 75, and 78 to 81 and five α-helices composed of residues 4 to 9, 24 to 34, 54 to 65, 83 to 91, and 94 to 100 in contrast to the three helices observed in *E. coli* glutaredoxin-1. The β-sheet forms the central core of the protein with helices 1 and 3 located on one side of the sheet and helices 2, 4, and 5 located on the other side. The structure is very similar to the determined X-ray crystallographic structure of oxidized pig liver glutaredoxin (Katti *et al*., 1995).

As seen in Figure 5a, the structure is very well-defined with several localized regions of increased disorder including the N-terminal Ala2 and Gln3 residues, around the active site Thr22 whose amide NH was not observable, and around Thr51 and Asn52, located in the loop before helix 3. In all cases, a very low density of NOE upper distance constraints was obtained in these regions (Figure 2). Measurement of the ^{15}N T_2 values (Figure 5b) for the backbone of the protein shows the active site Cys23 to have the fourth highest value, suggesting increased mobility in this region of the protein which appears to be reflected in the structures. Residues 51 and 52 display depressed T_2 values

Table 1. Analysis of the top 20 conformers before and after energy minimization with the program OPAL

Quantity	Average ± standard deviation (range)	
	Before energy minimization	After energy minimization
DYANA target function (Å^2)	1.50 ± 0.28 (1.1 . . . 2.2)	
AMBER energy (kcal/mol)	−6686.3 ± 168.5 (−6998.9 . . . −6270.4)	−9972.6 ± 140.2 (−10198.6 . . . −9649.1)
Residual distance constraint violations		
Sum (Å)	8.23 ± 0.88 (6.85 . . . 10.02)	9.78 ± 0.46 (8.92 . . . 10.74)
Maximum (Å)	0.29 ± 0.08 (0.22 . . . 0.53)	0.10 ± 0.01 (0.10 . . . 0.12)
Residual dihedral angle constraints violations		
Sum (deg.)	24.3 ± 6.1 (16.4 . . . 38.8)	45.8 ± 4.7 (37.1 . . . 55.5)
Maximum (deg.)	4.3 ± 1.4 (2.5 . . . 8.0)	2.5 ± 0.3 (2.1 . . . 3.2)

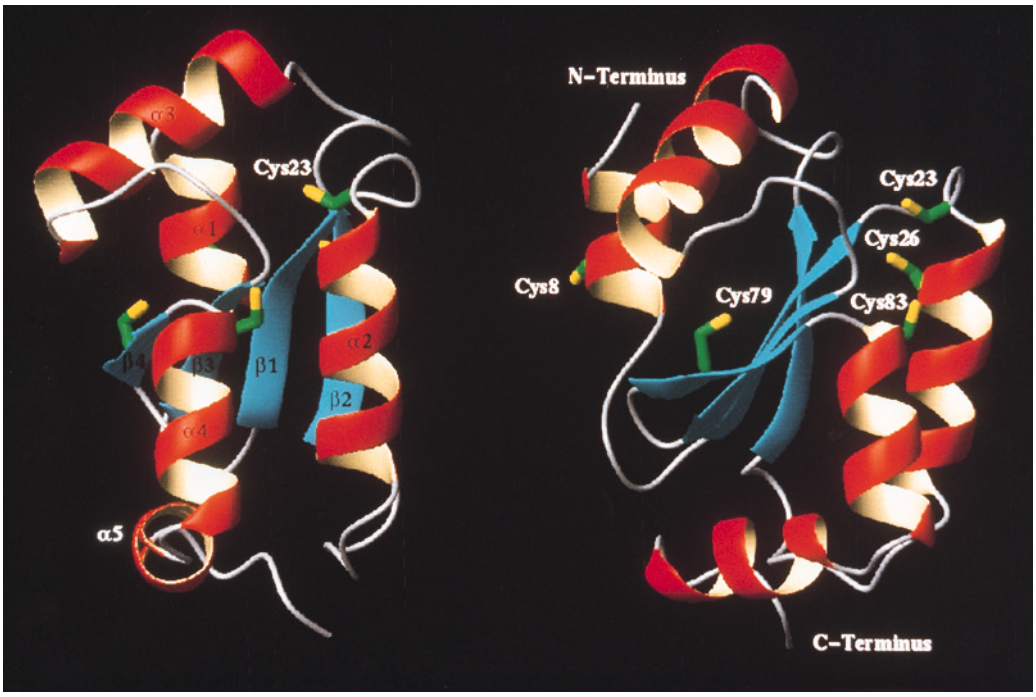

Figure 3. Two views of a ribbon representation of human glutaredoxin in the fully reduced form. The drawing was produced with the program MOLMOL (Koradi *et al.*, 1996). The helices are colored red and yellow, the β-strands cyan, and other segments gray. Cys23 and the secondary structure elements are indicated on the left. The right view represents a 60° rotation around the vertical axis relative to the left panel and all the Cys residues are illustrated.

relative to the bulk of the protein possibly indicating conformational exchange for this portion of the protein. Interestingly, residues in the corresponding loop in *E. coli* glutaredoxin-1 have been shown to undergo significant changes in their dynamic behavior between the oxidized and reduced forms of *E. coli* glutaredoxin-1 (Kelley *et al.*, 1997). This loop has also recently been identified as playing a

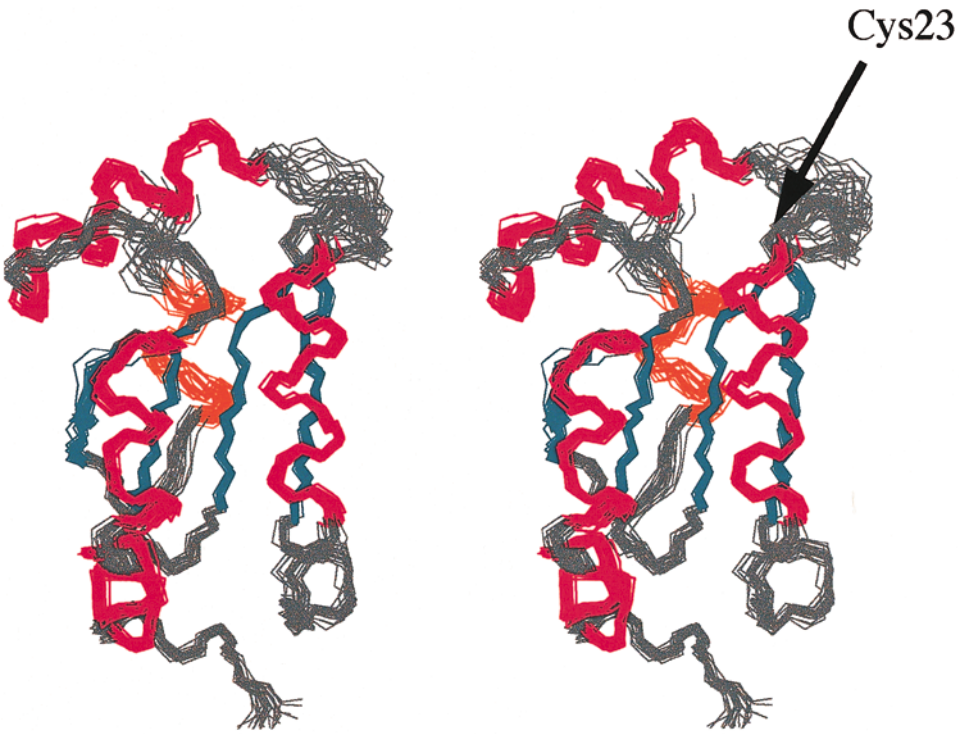

Figure 4. Stereo view of the backbone of the 20 conformers representing the solution structure of fully reduced human glutaredoxin. The α-helices, β-strands, and other segments are colored red, dark cyan, and gray, respectively. The protein orientation corresponds to that in the left panel of Figure 3. The active site is indicated with an arrow.

Table 2. Average RMSD values between the 20 final energy-minimized conformers and their average coordinates

Atoms used for the comparison	RMSD (Å) ± standard deviation
Backbone atoms N, C^{α}, C′ of all residues (2 to 106)	0.54 ± 0.08
All heavy atoms (2 to 106)	1.01 ± 0.08
Backbone atoms of regular secondary structure elements[a]	0.41 ± 0.07
All heavy atoms of regular secondary structure elements[a]	0.87 ± 0.08

The average coordinates were calculated after superposition of the 20 conformers for minimal RMSD of the backbone atoms of residues 2 to 106.

[a] Secondary structure elements include the following residues: 4 to 9, 24 to 34, 54 to 65, 83 to 91, 94 to 100 for helices, and 15 to 19, 43 to 47, 72 to 75, 78 to 81 for β-strands.

role in the binding of *E. coli* glutaredoxin-1 to ribonucleotide reductase (Berardi *et al.*, 1998). We were not able to obtain ^{15}N T_2 measurements for the N-terminal Ala2 and Gln3 residues due to the absence of these NH resonances from the spectra.

In addition to the characteristic i to $i + 4$ hydrogen bonds in the helices and the inter-strand hydrogen bonds observed between the residues of the β-sheet, a number of structurally important hydrogen bonds have been identified. In the active site, the HN of Agr27 is hydrogen-bonded to the CO of Cys23 to provide a turn that is important for the positioning of the active site cysteine residues as well as for initiation of α-helix 2. A hydrogen bond between the NH of Lys39 and the CO of Ala104 serves to hold α-helix 5 in contact with the extended loop between α-helix 2 and β-strand 2. In *E. coli* glutaredoxin-1, there is no α-helix 5 and the loop between α-helix 2 and β-strand 2 is much shorter, thus the extended nature of this loop is apparently necessary for interactions with α-helix 5. A consistent hydrogen bond is observed from the NH of Thr49 to the side-chain carboxylate of Asp47. As mentioned above, the loop containing Thr49 has been shown to be important in the binding of *E. coli* glutaredoxin-1 to ribonucleotide reductase (Berardi *et al.*, 1998); thus, this hydrogen bond is likely to be important for the determination of the conformation of this loop. The side-chain NH_2 of Gln58 shows a consistent hydrogen bond to the CO of Arg68 which is important for the placement of α-helix 3 on the core of protein. A hydrogen bond between the side-chain OH of Thr65 to the CO of Leu61 serves as a C-terminal helix cap that will help to stabilize the C-terminal end of α-helix 3. Both this hydrogen bond and the previous one are located in close proximity to the site of binding of glutathione (Bushweller *et al.*, 1994) and of ribonucleotide reductase (Berardi *et al.*, 1998) identified in *E. coli* glutaredoxin-1, suggesting that their presence or absence could be influenced by substrate binding and could provide a mechanism for conformational changes associated with binding. Helices 4 and 5 are bent at an angle of approximately 90° to one another. This break occurs at Gly93 where two hydrogen bonds help to stabilize this kink: HN of Leu95 to CO of Leu89 and HN of Leu96 to CO of Gly93.

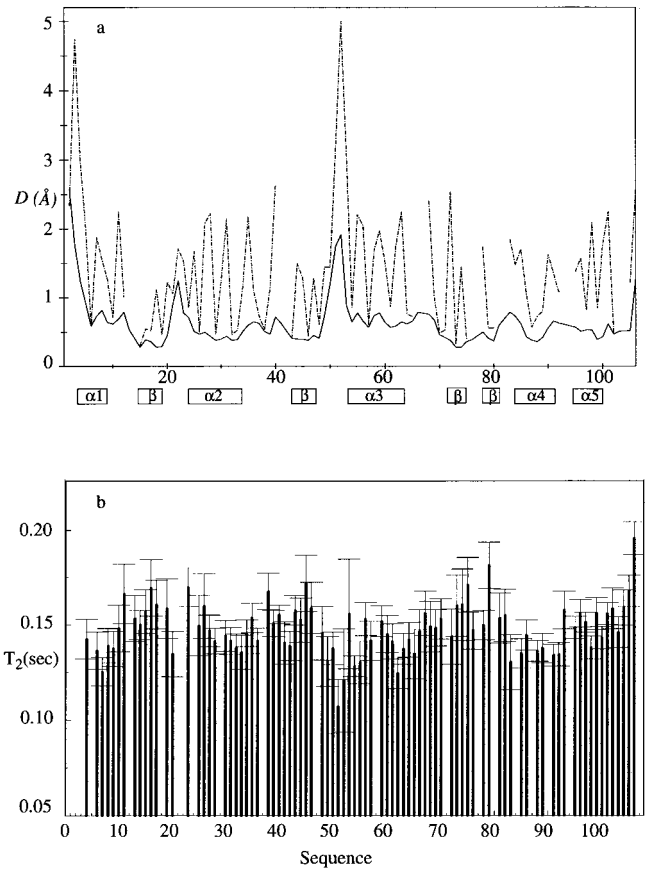

Figure 5. a, Plot of average global displacement *versus* the sequence calculated either for the backbone atoms N, C^{α} and C′ (continuous line) or the side-chain heavy atoms (broken line) of the 20 conformers of reduced human glutaredoxin relative to the mean coordinates. b, Plot of ^{15}N T_2 values as a function of the resolved backbone NH groups in fully reduced human glutare-

Discussion

Comparison of reduced human glutaredoxin to related structures

Comparison of the *E. coli* glutaredoxin-1 (Sodano *et al.*, 1991) and human glutaredoxin structures shows the fold of *E. coli* glutaredoxin-1 to be well preserved in the structure of human glutaredoxin with several notable changes. The RMSD between the *E. coli* and human glutaredoxins is 1.0 Å for the residues listed in Table 3, indicating very close

Table 3. Backbone RMSD between the solution structure of reduced human glutaredoxin, reduced form of *E. coli* glutaredoxin-1, reduced form of human thioredoxin, and the crystal structure of oxidized pig liver glutaredoxin

	Human Grx ⟨Red⟩	Pig Grx Ox	*E. coli* Grx-1 ⟨Red⟩
Pig Grx Ox	0.6		
E. coli Grx-1 ⟨Red⟩	1.0	1.0	
hu Trx Red	1.6	1.5	1.9

Averaged coordinates of 20 NMR conformers were used for human glutaredoxin and reduced *E. coli* glutaredoxin-1 (Sodano *et al.*, 1991; Protein Data Bank entry 1EGR) in this Table, which are indicated as human Grx ⟨Red⟩ and *E. coli* Grx-1 ⟨Red⟩. X-ray structures of pig liver glutaredoxin (Katti *et al.*, 1995; Protein Data Bank entry 1KTE) and reduced human thioredoxin (Weichsel *et al.*, 1996; Protein Data Bank entry 1ERT) are represented as Pig Grx Ox and hu Trx Red, respectively. Thirty-three residues were used to align the structures and calculate the displacements for the backbone atoms N, C^{α}, and C′ in this Table, which are residues 15 to 19, 23 to 35, 43 to 47, 72 to 75, and 78 to 83 for human glutaredoxin; residues 14 to 18, 22 to 34, 42 to 46, 71 to 74, and 77 to 82 for pig liver glutaredoxin; residues 3 to 7, 11 to 23, 33 to 37, 61 to 64, and 67 to 72 for *E. coli* glutaredoxin-1; and residues 24 to 28, 32 to 44, 55 to 59, 76 to 79, and 87 to 92 for human thioredoxin.

agreement of the structures for this portion of the protein. The human glutaredoxin contains two additional helices relative to its *E. coli* counterpart located at the N and C termini of the protein. The loop connecting α-helix 2 to β-strand 2 (α1 to β2 in *E. coli*) is substantially longer in the human protein. The helix containing the active site is one turn shorter in the human protein, perhaps also contributing to the increased length of the aforementioned loop. In addition, α-helix 3 in human glutaredoxin is one turn longer and positioned differently than its counterpart in *E. coli* glutaredoxin-1. This results in a narrowing of the groove into which the ribonucleotide reductase substrate has been shown to bind in *E. coli* glutaredoxin-1 (Berardi *et al.*, 1998). The narrowing of this groove is quite interesting in light of the fact that the corresponding region of the human ribonucleotide reductase, which presumably binds in the same region, contains residues which are much smaller in size than those in the *E. coli* ribonucleotide reductase.

Comparison of the human glutaredoxin structure to the X-ray crystal structure of oxidized pig liver glutaredoxin (Katti *et al.*, 1995) shows very good agreement with an RMSD of overall backbone atoms of 1.2 Å and a value of 0.6 Å for the residues indicated in Table 3. However, there are several notable differences. Figure 6 shows a plot of the backbone displacement between the mean structure of human glutaredoxin and the X-ray structure of pig liver glutaredoxin as well as the average *B*-factors of backbone N, C^{α}, and C′ atoms from the X-ray structure of pig liver glutaredoxin (numbering used is based on human glutaredoxin, starting from Ala2). The loop following α-helix 2 shows a significant displacement between the two proteins. As seen in Figure 6, only residue 35 (Glu34 in pig liver) shows an increased *B*-factor for this loop; thus, this appears to be a real difference between the two structures. Because this loop is in contact with α-helix 5, there is also a displacement in the position of α-helix 5 resulting from this difference. Examination of the crystal structure of pig liver glutaredoxin shows Glu39 (Gln40 in human Grx) forming an intermolecular salt bridge with residue Arg97 (Arg98 in human Grx) in another protein molecule. This crystal packing interaction provides an explanation for the differences observed between the two structures in these regions. In addition, residues Asn52 to Thr54 (corresponding to Ser51 to Thr53 in pig liver glutaredoxin) in the loop following β-strand 2 also displays a significant displacement between the two structures. As mentioned above, this is a region of the protein where the solution structure is not well defined due to a low density of constraints. As also mentioned above, the ^{15}N T_2 values for Thr51 and Asn52 display depressed values potentially indicative of conformational exchange in this region. Consistent with this, the pig liver structure shows increased *B*-factors for this region of the structure.

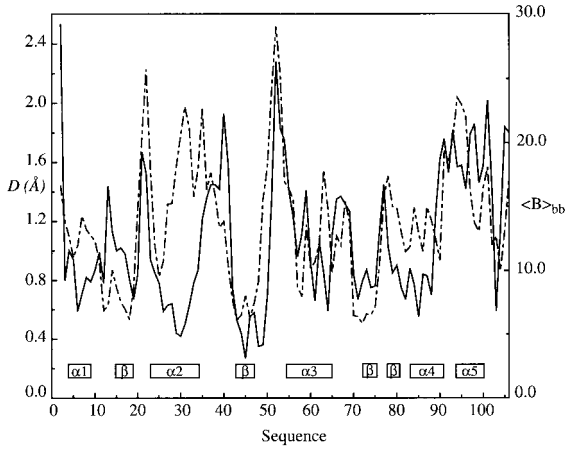

Figure 6. Continuous line: plot of the displacement of the backbone atoms N, C^{α} and C′ between the mean structure of reduced human glutaredoxin and the X-ray structure of oxidized pig liver glutaredoxin (Katti *et al.*, 1995). Broken line: the average *B* factors of the backbone N, C^{α} and C′ atoms in oxidized pig liver glutaredoxin (Katti *et al.*, 1995).

Comparison with the X-ray crystal structure of reduced human thioredoxin (Weichsel *et al.*, 1996) shows good agreement between the two proteins for the four-stranded β-sheet (β2 to β5) and for helix 2 of human glutaredoxin which give an RMSD of 1.6 Å (Table 3). Human thioredoxin contains an additional β-strand at its N terminus that combines to form a five-stranded β-sheet. In addition, α-helix 4 in human glutaredoxin is replaced by an extended secondary structure element in human thioredoxin. This is likely to be functionally important since corresponding residues in this helix have been implicated in the binding of glutathione (Bushweller *et al.*, 1994) as well as ribonucleotide reductase (Berardi *et al.*, 1998) to *E. coli* glutaredoxin-1. The removal of this helix creates a much less tortuous surface than that found in glutaredoxins which may help to explain the enhanced substrate specificity glutaredoxins display relative to thioredoxins which are quite general protein disulfide reductases.

Environment of the active site

The pK_a value of the active site thiol in glutaredoxins has been shown to have a dramatically depressed value of ca. 4.5 (Björnberg, 1990; Gan & Wells, 1987b; Mieyal *et al.*, 1991), indicating that it will exist as a thiolate anion at physiological pH. In order to account for the presence of this thiolate, the OPAL energy minimizations have been carried out with Cys23 in the thiolate form. Comparison of energy minimizations with the thiol and thiolate forms of Cys23 showed that there is a substantive effect of this change in terms of the local structure in the active site region. Figure 7 shows a plot of the displacement between the mean coordinates of the conformers minimized with a thiol or thiolate at Cys23. There are clear differences in the two structures for backbone and side-chain nuclei in the vicinity of the active site and more modest changes for a number of side-chains located elsewhere. The most dramatic side-chain movement occurs for Lys20, which is conserved as a positive charge in all the known glutaredoxins, suggesting an important role for this residue in glutaredoxins' function. In addition, the side-chains of Arg27, Arg68, and Arg98 move more modestly in response to the change in electrostatic field associated with having a thiolate at this position. Changes in the backbone and side chain conformation in the vicinity of the active site also result in a different pattern of interactions observed in the vicinity of the active site (see Table 4).

The stabilization of this negative charge on Cys23 has been proposed to arise from a variety of influences including the dipole moment of the

Table 4. Interactions identified in the active site region after SH and S^- energy minimization

	No. of conformers SH	S^-
Hydrogen bond interactions		
C26 $H^N \rightarrow$ C23 O'[a]	15	2
R27 $H^N \rightarrow$ C23 O'[a]	7	14
C26 $H^N \rightarrow$ C23 S^γ[b]	9	10
C26 $H^\gamma \rightarrow$ C23 S^γ[b]	6	13
Y25 $H^N \rightarrow$ C23 S^γ[b]	13	9
Electrostatic interactions[c]:		
C23 $S^\gamma \rightarrow$ K20 H_3N^ζ	2 (3.2–3.4 Å)	4 (<3.0 Å)

The 20 energy minimized conformers were examined with the program XAM for possible hydrogen bonding or electrostatic interactions.

[a] A hydrogen bond was identified if the proton-acceptor distance was less than 2.4 Å, the angle between the donor-proton bond and the line connecting the donor and acceptor atoms was less than 35°. The No. of conformers column lists the number of conformers each of the hydrogen bonds was observed in.

[b] Hydrogen bonds involving sulfur were identified if the proton-acceptor distance was less than 3.2 Å.

[c] An electrostatic interaction was identified when two charged functional groups were separated by less than 3.5 Å. The numbers in parentheses indicate the distance between the charged groups for identified conformers.

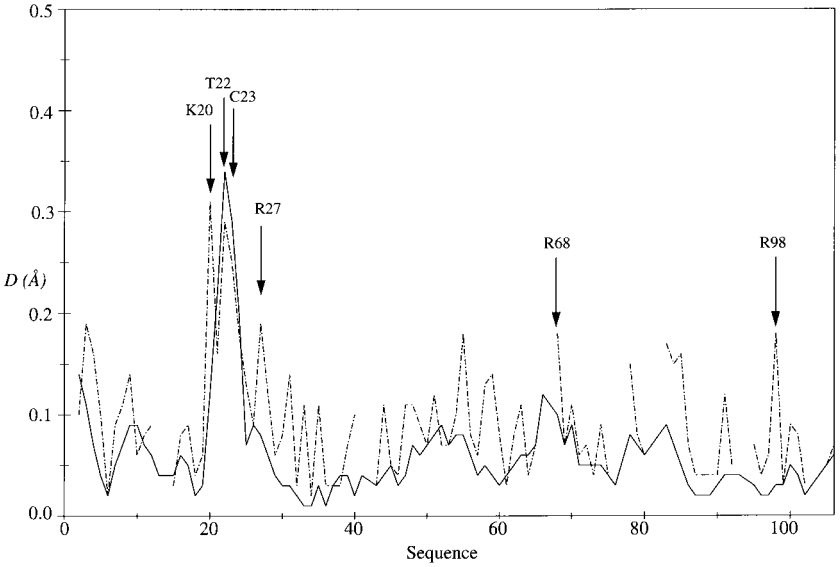

Figure 7. Plot of the displacement of the backbone atoms N, C^α and C′ (continuous line) and the side-chain heavy atoms (broken line) between the mean structures of reduced human glutaredoxin energy minimized with Cys23 as the thiol (SH) or as the thiolate (S^-). The arrows indicate substantial displacements observed between the two.

active site helix (Hol, 1985; Katti *et al*., 1990; Gane *et al*., 1995; Kortemme & Creighton, 1995), hydrogen bonding between active site thiols (Jeng *et al*., 1995), hydrogen bonding between the N-terminal Cys S^{γ} and the amide proton of the more C-terminal active-site Cys (Katti *et al*., 1990; Forman-Kay *et al*., 1992; Eklund *et al*., 1992; Sun *et al*., 1997), and electrostatic interactions between the thiolate anion and positively charged residues in the active site region (Lundstrom-Ljung *et al*., 1992; Kortemme *et al*., 1996). In order to address this question, we have calculated the electrostatic potential on the surface of the protein using QUANTA97 (QUANTA, Molecular Simulations Inc.). Figure 8 shows the results of this calculation. The thiol of Cys23 is located in a region of substantial positive potential as has also been observed for *E. coli* glutaredoxin-1 (Berardi *et al*., 1998). In order to assess what specific interactions may be responsible for the stabilization, we have also examined the structures for interactions with the thiolate anion. Hydrogen bond interactions were identified in nine or more of the conformers between the thiolate anion and the HN of Tyr25, the HN of Cys26, and the SH of Cys26 (Table 4). Interaction with the NH of Cys26 is consistent with the dramatic downfield shift of the NH resonance of the corresponding cysteine observed upon going from the oxidized to the reduced form in *E. coli* Grx-1. The interaction with the SH of Cys26 is interesting in that it implies a sharing of this proton between the two thiols which has also been proposed for *E. coli* thioredoxin (Jeng *et al*., 1995). This would fit with the results of mutagenesis data which show that replacement of the more C-terminal Cys in the active site with a Ser in pig liver glutaredoxin results in a protein which retains all of its GSH disulfide oxidoreductase activity whereas mutation of this residue to an Ala results in a loss of 91% of its activity (Yang & Wells, 1991). The distance between Cys23 S^{γ} and Cys26 S^{γ} observed in human Grx is 4.1(±0.8) Å, which is close to that seen in the NMR structure of reduced *E. coli* Trx (3.82 Å; Jeng *et al*., 1994) and in the X-ray structure of reduced wild-type human Trx (3.9 Å; Weichsel *et al*., 1996). In contrast, the corresponding distance in the NMR structure of a mutant human Trx was observed to be 3.1 Å (Qin *et al*., 1994). The side-chain ammonium group of Lys20 was also observed within 3.0 Å of the sulfur of Cys23 in four of the 20 conformers, suggesting that this residue may also contribute to the local positive electrostatic potential. The positive charge at this position is conserved across all known glutaredoxins. As the pK_a value of the glutaredoxin nucleophilic thiol is substantially lower than that for thioredoxin, the additional interactions observed with the thiolate in human glutaredoxin may account for the significantly lower pK_a observed for Grx relative to Trx.

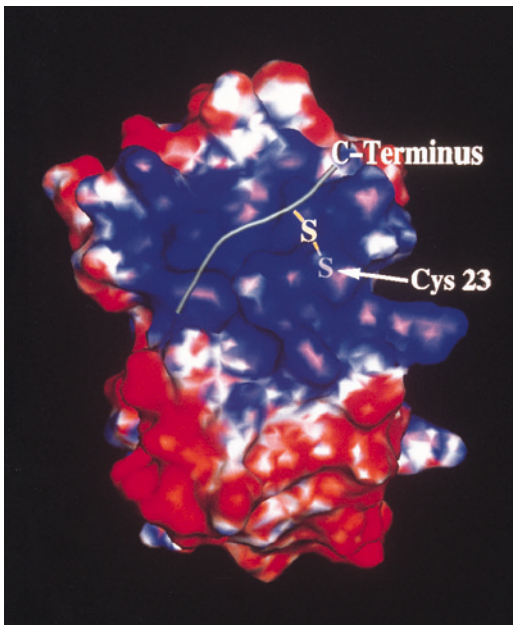

Figure 8. Electrostatic potential of reduced human glutaredoxin calculated with Cys23 as a thiolate anion mapped on a surface defined with a 1.4 Å probe. The protein orientation corresponds to the left panel of Figure 2. Blue areas correspond to positively charged regions and red areas to negatively charged regions. QUANTA97 (QUANTA, Molecular Simulations Inc.) was used for the calculation. The binding orientation for the peptide corresponding to the C terminus of human ribonucleotide reductase obtained from the molecular dynamics is schematically represented by a grey rod using the C^{α} trace of the C-terminal nine residues of the peptide. For clarity, the disulfide linkage is shown; however, the electrostatic potential displayed is for the Cys23 thiolate anion form of the free protein.

In order to assess the generality of this local electrostatic potential determining the pK_a value of the Cys residues in these proteins, we have calculated the electrostatic potential at the nucleophilic sulfur for *E. coli* glutaredoxin-1, *E. coli* thioredoxin, and *E. coli* DsbA for which the pK_a values have been determined (Björnberg, 1990; Kallis & Holmgren, 1980; Nelson & Creighton, 1994). As shown in Table 5, there is a good correlation between the calculated potential and the observed pK_a value, indicating that this is an effective predictor of the thiol pK_a value. The somewhat poor agreement for *E. coli* DsbA may result from the use of the oxidized structure for the calculations. Clearly, the unusually low pK_a values observed for the nucleophilic thiols of Grx and Trx arise not from a single interaction but from the sum of a number of interactions. Calculation of the local electrostatic potential takes all of these effects into account and is therefore a general tool for evaluating charge stabilization of thiolate anions or any other ionizable groups.

As mentioned above, the active site nucleophilic thiol is located in a region of positive electrostatic potential on the protein. This has also recently been identified as the binding site for both GSH (Bushweller *et al*., 1994) and ribonucleotide reductase (Berardi *et al*., 1998) on *E. coli* glutaredoxin-1. As seen in the case of *E. coli*, the C-terminal end of the B1 subunit of human ribonucleotide

Table 5. Comparison between electrostatic potential at nucleophilic Cys sulfur atom and corresponding pK_a values in reduced human glutaredoxin, reduced *E. coli* glutaredoxin-1, reduced *E. coli* thioredoxin, and *E. coli* DsbA

	Human Grx	*E. coli* DsbA[a]	*E. coli* Grx-1	*E. coli* Trx
$\langle E_{pot} \rangle$ (kcal/mol)	29.6	10.9	15.7	1.1
pK_a[b]	3.8	3.5	4.5	6.7

The average electrostatic potentials at the sulfur atom on the Connolly surface of the nucleophilic Cys residues were calculated with QUANTA97 (QUANTA, Molecular Simulations Inc.) The X-ray structure of oxidized *E. coli* DsbA (Martin *et al*., 1993; Protein Data Bank entry 1DSB), the lowest energy conformer of the NMR solution structure of reduced *E. coli* thioredoxin (Jeng *et al*., 1994; Protein Data Bank entry 1XOB), and the lowest energy conformer of the NMR solution structure of reduced *E. coli* glutaredoxin-1 (Sodano *et al*., 1991; Protein Data Bank entry 1EGR) were used to calculate the electrostatic potential. The lowest energy conformer of the 20 energy-minimized human glutaredoxin conformers with Cys23 as protonated thiol (SH) was used for the calculation.

[a] Oxidized X-ray crystal structure of *E. coli* DsbA has been used for this calculation.

[b] The pK_a values for human Grx, *E. coli* DsbA, *E. coli* Grx-1, and *E. coli* Trx were obtained from Mieyal *et al*. (1991), Nelson & Creighton (1994), Björnberg (1990) and Kallis & Holmgren (1980), respectively.

reductase possesses a negative overall charge which will be attracted to the positive potential located in the vicinity of the active site on human glutaredoxin. Also as seen in the case of *E. coli* glutaredoxin-1 (Berardi *et al*., 1998), the overall dipole moment of human glutaredoxin extends directly through the active site in such a manner that it will tend to guide negatively charged disulfide substrates such as the C terminus of ribonucleotide reductase B1 or glutathione containing mixed disulfides down into the active site, thereby enhancing the on-rate for the reaction.

Role of the additional Cys residues

All of the mammalian thioredoxins and glutaredoxins have been shown to contain additional Cys residues to those located in the active site. Mutagenesis of Cys78 and Cys82 in pig liver glutaredoxin (Cys79 and Cys83 in human Grx) did not perturb the ability of the protein to reduce small-molecule GSH mixed disulfides or ascorbate to any significant extent (Yang & Wells, 1991). Because these mutants have not been assayed for their effect on protein disulfide reduction, the exact role of the additional cysteine residues in mammalian glutaredoxin has not been established. However, their spatial location and local environment may provide hints as to possible functional importance. Cys8 is located in the N-terminal helix and is solvent-exposed. The presence of this Cys decreases the lifetime of human glutaredoxin samples considerably with substantial aggregation of the protein if it is not maintained in a fully reduced state. The corresponding Cys8 → Ser mutation significantly improves this behavior (Padilla *et al*., 1996). Formation of disulfide-linked aggregates of human Grx is interesting in light of the recent demonstration that human thioredoxin can form disulfide-linked dimers *in vitro* which inhibit the activity of the protein (Weichsel *et al*., 1996). Dimerization or oligomerization of human Grx with disulfide cross-linking may also have a role in the regulation of human glutaredoxin, since oxidation has been shown to inhibit the activity of calf thymus glutaredoxin (Klintrot *et al*., 1984). Cys79 is located in β-strand 4 and is also solvent-exposed, perhaps also providing a site for oligomerization. Cys83 is located at the N-terminal end of α-helix 4 which has been shown to be an important site for binding of GSH to *E. coli* glutaredoxin-1 (Bushweller *et al*., 1994). It is solvent-exposed and is located in a region of positive electrostatic potential (see Figure 8), suggesting it will have a depressed pK_a value and will be likely to be active in redox reactions. The proximity of this residue to the active site, its location in the GSH binding site, and the local electrostatic potential strongly suggest a key role for this thiol in the regulation of the protein or in one or more of the known activities of the protein.

Modeling of GSH and ribonucleotide reductase B1 binding sites on human glutaredoxin

In order to model the binding of glutathione and the B1 subunit of ribonucleotide reductase to human glutaredoxin, we have carried out molecular dynamics simulations of mixed disulfides between human Grx and either glutathione or a 16 residue peptide corresponding to the C terminus of the B1 subunit of human ribonucleotide reductase. The choice of the length of peptide utilized and the cysteine to form the mixed disulfide with was based on a recent study utilizing *E. coli* Grx-1 and a peptide derived from the C terminus of the *E. coli* ribonucleotide reductase which showed the more C-terminal cysteine to be the site of nucleophilic attack by Grx-1 and approximately ten C-terminal residues to be in direct contact with the protein (Berardi *et al*., 1998). The initial starting conformation for the glutathione simulation placed the glutathione in the orientation observed in the NMR solution structure of the mixed disulfide between *E. coli* Grx-1(C14S) and glutathione (Bushweller *et al*., 1994). The initial orientation chosen for the peptide places the C-terminal end of the peptide in a similar location to the C-terminal Gly in the glutathione model and is based on the recent preparation and characterization of a mixed

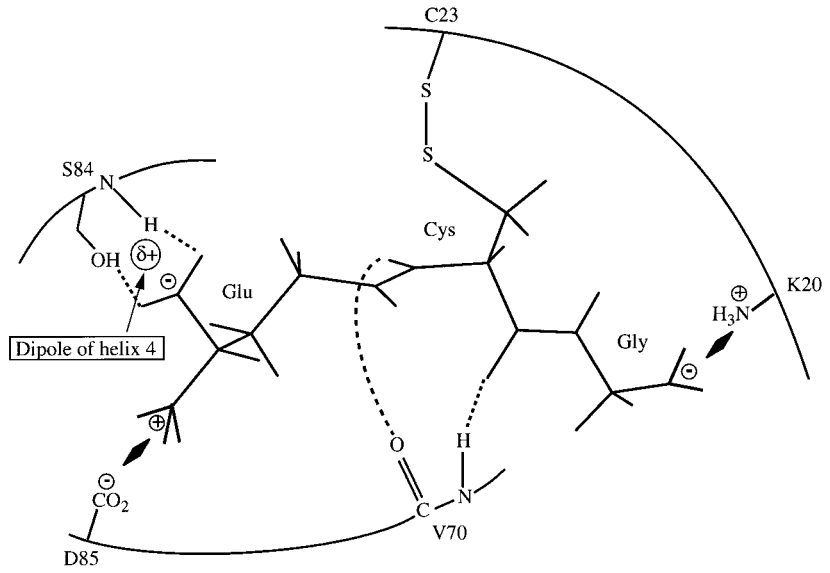

Figure 9. Schematic of the interactions predicted between glutathione and human glutaredoxin in ten or more of the 20 conformers obtained from the molecular dynamics simulation. Hydrogen bonds are illustrated with broken lines and electrostatic interactions with filled diamonds. The circle with the δ+ inside identifies the location of the N-terminal end of helix 4.

disulfide between *E. coli* Grx-1(C14S) and a 25 residue peptide corresponding to the C terminus of *E. coli* ribonucleotide reductase B1 (Berardi *et al.*, 1998).

Figure 9 shows the interactions that have been identified between glutathione and human glutaredoxin in a majority of the conformers analyzed from the molecular dynamics simulation. Both the location and the interactions predicted are very similar to those seen in the mixed disulfide between *E. coli* glutaredoxin-1 and glutathione (Bushweller *et al.*, 1994). As seen in the *E. coli* system, the charged functionalities of the γ-Glu residue are predicted to be located at the N-terminal end of α-helix 4 in human glutaredoxin with electrostatic interactions between the ammonium group and the conserved Asp at position 85 as well as between the carboxylate and the helix dipole of α-helix 4. Hydrogen bonds between the NH and OH of Ser84 and the carboxylate of γ-Glu are also predicted as was observed in the *E. coli* system (Bushweller *et al.*, 1994). The carboxylate of the Gly residue in glutathione is predicted to form an electrostatic interaction with Lys20, unlike the interaction observed in the *E. coli* system. Lys20 is conserved as a positive charge across all the glutaredoxins, suggesting functional importance for this interaction. In the *E. coli* system, this interaction involves Lys45 which is an Asp in the human protein. The MD simulation also predicts hydrogen bonds between the CO and NH of Val70 and the NH and CO of the cysteine in the glutathione, respectively. The Val70 NH to Cys CO hydrogen bond was also identified in the *E. coli* system; however, the Val70 CO to Cys NH hydrogen bond was not observed in a majority of the conformers (Bushweller *et al.*, 1994).

The simulation of the human Grx-peptide mixed disulfide proved quite revealing in terms of functional understanding of the interactions between the two. The peptide binds in a groove located on the surface of the protein in the vicinity of the active site (Figure 8). Figure 10 shows the predicted interactions between the protein and the peptide identified in a majority of the ten representative conformers analyzed. A number of the interactions predicted in the complex with glutathione have parallels in this complex. The ammonium group of Lys20 is predicted to interact with the C-terminal carboxylate of Ser792. A hydrogen bond is predicted between the Val70 CO of human Grx and the Cys787 NH of the peptide. The MD results also predicted an electrostatic interaction between the conserved Asp85 in human Grx and Arg784 in the peptide. In addition, a hydrogen bond was predicted between the Cys83 NH of human Grx and the carboxylate of Glu786 in the peptide as well as an electrostatic interaction between Arg72 of the protein and the carboxylate of Glu786 in the peptide. An electrostatic interaction is also predicted between Arg28 of the protein and Asp785 of the peptide. Interestingly, the positive charge at Lys20 and at Arg28 is highly conserved among glutaredoxins, suggesting a functional importance for these interactions. Arg72 is conserved among the mammalian glutaredoxins but not in the *E. coli* protein, which may be one source of binding specificity. Consistent with this, an alignment of the ribonucleotide reductase B1 sequences (Berardi *et al.*, 1998) shows Glu786 to be a Gly in the *E. coli* sequence. The hydrogen bond involving Cys83 is interesting from a regulatory point of view in that it is clear that oxidation of this thiol would have a substantial effect on binding to ribonucleotide reductase, thus providing further credence to the notion of this as a site for redox regulation. This residue is replaced by a Tyr in *E. coli* glutaredoxin-

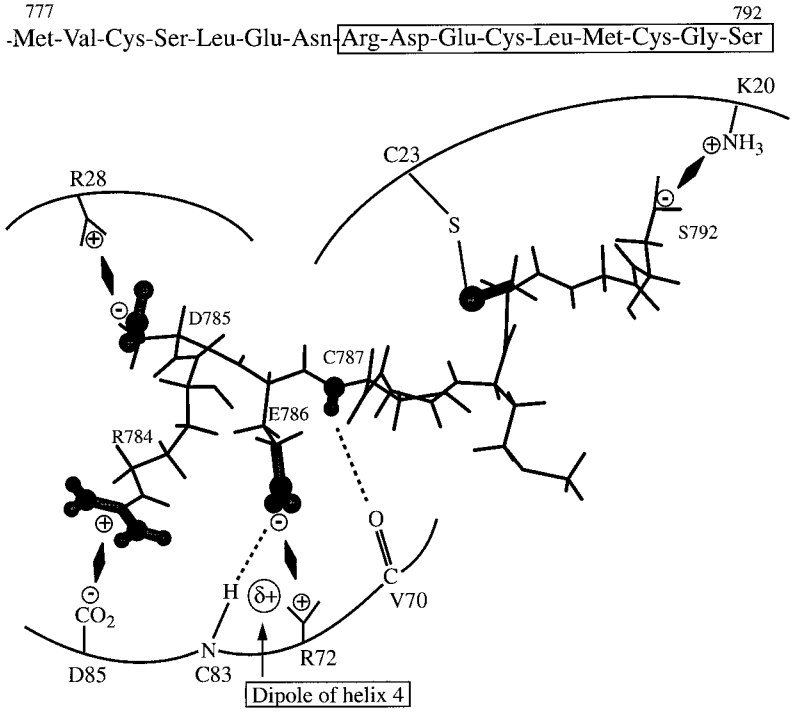

Figure 10. Schematic of the interactions predicted between human glutaredoxin and the peptide derived from human ribonucleotide reductase in five or more of the ten conformers obtained from the molecular dynamics simulation. The sequence of the peptide used in the simulation is shown at the top. Only the C-terminal nine residues, which show interactions with the protein are drawn, as indicated with a box. Hydrogen bonds are illustrated with broken lines and electrostatic interactions with filled diamonds. The circle with the δ+ inside identifies the location of the N-terminal end of helix 4.

1 which may also help to determine substrate specificity in these proteins.

Materials and Methods

Sample preparation

Uniformly ^{15}N and $^{13}C/^{15}N$-labeled human glutaredoxin samples (0.8 mM and 1.8 mM, respectively) were prepared as described (Sun *et al.*, 1997). The proteins were exchanged into a buffer of 50 mM potassium phosphate (pH 6.0), 0.1 mM EDTA, 5 mM DTT, 0.1% NaN_3, 95% $H_2O/5\%$ ^2H_2O or 100% ^2H_2O.

NMR spectroscopy

NMR measurements were carried out at 30°C on a Varian Unityplus 500 MHz NMR spectrometer equipped with an actively shielded triple resonance probe (Nalorac Corporation) and pulsed field gradients. Pulsed field gradients were utilized for suppression of the water signal and undesired coherence pathways (Bax & Pochapsky, 1992; Wider & Wüthrich, 1993). NMR data were processed with the program PROSA (Güntert *et al.*, 1992) and the resulting NMR data were visualized and analyzed using the program XEASY (Bartels *et al.*, 1995).

For collection of NOE upper distance constraints, 3D ^{13}C-edited (Muhandiram *et al.*, 1993) and ^{15}N-edited NOESY (Zhang *et al.*, 1994) spectra were recorded with a 60 ms mixing time on the 1.8 mM $^{13}C/^{15}N$-labeled sample in 95% $H_2O/^2H_2O$. Two separate ^{13}C-edited NOESY spectra were recorded with the ^{13}C carrier positioned at 43 ppm for aliphatic carbon atoms and at 132.3 ppm for the aromatic carbon atoms. Values of the $^3J_{HNH\alpha}$ vicinal coupling constants were derived from inverse Fourier transformation of in-phase multiples from a 2D [^{15}N,^1H]-COSY experiment (Szyperski *et al.*, 1992) and a 3D HNHA experiment (Kuboniwa *et al.*, 1994). Values of $^3J_{H\alpha H\beta}$ coupling constants were determined from a 3D HACAHB-COSY experiment recorded in ^2H_2O solution as described (Grzesiek *et al.*, 1995). In addition, vicinal $^3J_{NH\beta}$ coupling constants were estimated from a 3D HNHB experiment (Archer *et al.*, 1991). The number of complex points and acquisition times for these experiments was as follows: ^{15}N-NOESY, ^{15}N (F1), 32 complex points, 19.5 ms; ^1H (F2), 128 complex points, 19.6 ms; ^1H (F3), 512 complex points, 78.8 ms; ^{13}C-NOESY, ^{13}C (F1), 40 complex points, 9.9 ms; ^1H (F2), 124 complex points, 19.0 ms; ^1H (F3), 512 complex points, 78.8 ms; [^{15}N,^1H]-COSY, ^{15}N (F1), 192 complex points, 119 ms; ^1H (F2), 1024 complex points, 157.5 ms; HNHA, ^{15}N (F1), 28 points, 16.7 ms; ^1H (F2), 64 complex points, 11.3 ms; ^1H (F3), 512 complex points, 78.8 ms; HACAHB, ^{13}C (F1), 64 complex points, 15.7 ms; ^1H (F2), 64 complex points, 12.7 ms; ^1H (F3), 512 points, 102.4 ms; HNHB, ^{15}N (F1), 32 complex points, 19.2 ms; ^1H (F2), 64 complex points, 9.8 ms; ^1H (F3), 512 complex points, 78.8 ms.

For measurement of ^{15}N T_2 values, the pulse sequence by Farrow *et al.* (1994) optimized for minimal saturation of water was employed. A recycle delay of 1.0 second was used between acquisitions to ensure sufficient recovery of NH magnetization (Sklenar *et al.*, 1987). ^{15}N T_2 values were determined from 12 spectra with values of the CPMG delay of 16.3, 32.6, 48.9, 65.2, 81.4, 97.7, 114.0, 130.3, 146.6, 162.9, 228.0 and 325.8 ms. In order to generate pure absorptive 2D line shapes, the N and P-type signals recorded for each t_1 point were stored separately in order to carry out the necessary addition and subtraction of FID's and 90° phase correction as described (Kay *et al.*, 1992). The necessary data manipulations were carried out using software written in-house. Analysis of the data to obtain the ^{15}N T_2 values was carried out as described (Kelley *et al.*, 1997).

Determination of the three-dimensional structure

Structure calculations were carried out *via* torsion angle dynamics using the program DANA (Güntert *et al.*, 1997). The input for the DYANA calculations consisted

of upper distance limits derived from NOESY cross-peak intensities using the program CALIBA (Güntert *et al*., 1991) and dihedral angle constraints from the program HABAS (Güntert *et al*., 1989) derived from a backbone conformational search using the intra-residual and sequential NOEs together with the spin-spin coupling constants $^3J_{HNH\alpha}$ and $^3J_{H\alpha H\beta}$. HABAS also provided stereospecific assignments for 16 β-methylene groups. Inclusion of the qualitative $^3J_{NH\beta}$ data from the HNHB experiment allowed stereospecific assignments to be obtained for an additional 13 β-methylene groups. Stereospecific assignment of the side-chain NH_2 groups of Asn and Gln was based on the intensities of intra-residual NH_2-γCH_2 or βCH_2 protons in the 60 ms NOESY data. No explicit hydrogen bond constraints have been utilized at any step in the calculations. Initial structures were calculated with DYANA from a preliminary data set. The resulting conformers with lowest target function were utilized to redefine the calibration parameters in CALIBA (Güntert *et al*., 1991), to assign additional peaks in the NOESY spectra, and to obtain additional stereospecific assignments using the program GLOMSA (Güntert *et al*., 1991). GLOMSA analysis provided stereospecific assignments for diastereotopic methyls of eight Val and Leu residues in the protein as well as for 15 additional diastereotopic groups. The cycle of calculations and additional assignments was repeated until the NOESY spectra were exhausted. The DYANA calculations were started with 50 random conformers. A total of 10,000 MD steps were employed with the first 20% of the steps at high temperature (Thigh = 8.0) followed by slow cooling during the remainder of the MD steps to a final temperature Tend = 0.0 followed by 1000 steps of conjugate gradient minimization.

Following the torsion angle dynamics calculations, the 20 conformers with the lowest target function values were subjected to energy minimization using the AMBER force field (Cornell *et al*., 1995) implemented in the program OPAL (Luginbühl *et al*., 1996). In order to carry out the calculations with a thiolate for Cys23, a cysteine residue with a negatively charged sulfur was added into the corresponding AMBER library. Pseudo-energy terms were utilized for distance constraints and dihedral angle constraints where violations of 0.1 Å or 2.5° correspond to an energy of $kT/2$. The energy minimization was carried out with the protein surrounded by a shell of water molecules of thickness 6 Å and employing a uniform dielectric constant for the electrostatic interactions. A total of 1500 steps of conjugate gradient energy minimization were utilized for each conformer. The resulting 20 energy minimized conformers were used to represent the solution structure of fully reduced human glutaredoxin.

Structure comparisons and analysis

The programs MOLMOL (Koradi *et al*., 1996), Midasplus (Ferrin *et al*., 1988) and QUANTA97 (QUANTA, Molecular Simulations Inc.) were utilized to visualize the structures. Superpositions and pairwise RMSD values for human Grx were calculated using the program XAM (Xia, 1992). The mean coordinates were calculated by superposition of 20 final conformers to yield a minimal RMSD for the backbone atoms followed by averaging of the coordinates of the corresponding atoms in the superimposed conformers. The quality of the structures was evaluated with the program PROCHECK (Laskowski *et al*., 1996).

Electrostatic potential surfaces were calculated using the commercial software package QUANTA97 (QUANTA, Molecular Simulations Inc.). Atomic radii and charges were obtained from the CHARMm 23.2 parameter file with a dielectric constant of 4 at 300 K. The conformer with the lowest energy was used in the electrostatic potential calculations. The electrostatic potential was mapped on a solid surface defined by a 1.4 Å probe. The electrostatic distribution was represented with shades of blue for positively charged regions of potential energy from 0 to 50 kcal/mol, and shades of red for negatively charged regions with energies between 0 and −50 kcal/mol. The molecular dipole moment was calculated in QUANTA97 using the lowest energy structure. A value of 203 D was obtained for the magnitude of the dipole moment.

Molecular dynamics simulations

The lowest energy conformer of the 20 final energy-minimized conformers of human glutaredoxin was selected for use in subsequent studies. All calculations were performed with CHARMm 23.2 (Brooks *et al*., 1983; Karplus & Petsko, 1990). All energy terms were computed. A distance dependent dielectric model and a non-bonded cutoff of 15.00 Å was employed. For modeling of glutathione and ribonucleotide reductase binding to human Grx, glutathione and a 16 residue peptide corresponding to the C-terminal end of the B1 subunit of human ribonucleotide reductase were constructed using the Sequence Builder and Molecular Editor modules from the QUANTA97 program (QUANTA, Molecular Simulations Inc.). The glutathione and peptide segments were generated in elongated conformations and then energy-minimized for 50 and 200 cycles, respectively, using the Steepest Descents method and then for an additional 50 and 100 cycles, respectively, using the Adopted Basis Newton Rapson method. A mixed disulfide was constructed between Cys23 of human Grx and glutathione for modeling of the glutathione binding site. Similarly, a mixed disulfide between Cys23 of human Grx and Cys790 of the peptide was constructed.

For modeling of the glutathione binding site, an initial orientation of the glutathione on human Grx was selected to correspond to that observed in the mixed disulfide between *E. coli* Grx-1 and glutathione (Bushweller *et al*., 1994). Other orientations of the glutathione on the protein were found to be much higher in energy and were not explored further. The mixed disulfide was energy-minimized for 100 cycles using the Steepest Descents method while holding the protein coordinates fixed. Subsequently, the constraints on the protein coordinates were released and energy-minimization using the Adopted Basis Newton Rapson method was applied for 100 cycles. The mixed disulfide was heated to 350 K using 350 cycles of 0.001 ps per cycle for a total of 0.35 ps at 1 K/cycle. Equilibration was run for 2 ps with a temperature RMS deviation of 5 K in the last picosecond. The system was then subjected to 20 ps of molecular dynamics. Subsequently, three cycles consisting of 50 ps of molecular dynamics followed by 3 ps equilibration were then performed for a total of 150 ps of MD simulation. This was followed by four cycles of heating to 1000 K and annealing to 300 K in 10 ps followed by 5 ps equilibration at 300 K. Finally, two cycles consisting of 50 ps of molecular dynamics followed by 2 ps of equilibration were performed. Conformers were selected at

0.5 ps intervals. Cluster analysis was performed on the resulting 200 conformers. Twenty clusters were obtained with an RMSD threshold of 0.81 Å. The lowest energy conformer of each cluster was selected and energy-minimized using 100 cycles of the conjugated gradient method. The 20 resulting conformers were used for the analysis of the glutathione mixed disulfide.

For the peptide mixed disulfide model, one conformer was generated using the orientation of the peptide recently identified in a mixed disulfide between *E. coli* Grx-1 and a peptide derived from *E. coli* ribonucleotide reductase B1 (Berardi *et al.*, 1998). The mixed disulfide was energy-minimized for 300 steps using the Steepest Descents method with fixed atomic coordinates for the protein. Subsequently, an additional 150 cycles of unconstrained energy-minimization was performed using the Adopted Basis Newton Rapson method. The minimized model was heated from 0 to 300 K over 600 cycles with 0.001 ps per cycle. Equilibration was run for 5 ps with a temperature RMS deviation of 3 K in the last picosecond. The system was then subjected to 20 ps of molecular dynamics. Five cycles consisting of 30 ps of molecular dynamics followed by 3 ps equilibrium at 300 K were then performed. In the last 100 ps, conformers were selected at 1 ps intervals. Cluster analysis yielded ten clusters with an RMSD threshold of 0.74 Å. The lowest energy conformer of each cluster was selected and minimized using 150 cycles of the conjugated gradient method yielding the ten energy-minimized conformers utilized for subsequent analysis.

Acknowledgment

We thank Mr Wayne Casey for his help in maintaining the NMR spectrometer. These studies were supported by funds from Dartmouth College.

References

Ahn, B. Y. & Moss, B. (1992). Glutaredoxin homolog encoded by vaccinia virus is a virion-associated enzyme with thioltransferase and dehydroascorbate reductase activities. *Proc. Natl Acad. Sci. USA,* **89**, 7060–7064.

Archer, S. J., Ikura, M., Torchia, D. A. & Bax, A. (1991). An alternative 3D NMR technique for correlating backbone ^{15}N with side chain H^{β} resonances in larger proteins. *J. Magn. Reson.* **95**, 636–641.

Bartels, C., Xia, T., Billeter, M., Güntert, P. & Wüthrich, K. (1995). The program xeasy for computer-supported NMR spectral-analysis of biological macromolecules. *J. Biomol. NMR,* **6**, 1–10.

Bax, A. & Pochapsky, S. S. (1992). Optimized recording of heteronuclear multidimensional NMR spectra using pulsed field gradient. *J. Magn. Reson.* **99**, 638–643.

Berardi, M. J., Pendred, C. L. & Bushweller, J. H. (1998). Preparation, characterization, and complete heteronuclear NMR resonance assignments of the glutaredoxin (C14S)-ribonucleotide reductase B1 737-761 (C754S) mixed disulfide. *Biochemistry,* **37**, 5849–5857.

Björnberg, O. (1990). Glutaredoxin from *Escherichia coli;* high level expression and characterization of the redox-active center. Master thesis, Korolinska Institutet.

Brooks, B. R., Bruccoleri, R. E., Olafson, B. D., States, D. J., Swaminathan, S. & Karplus, M. (1983). CHARMM: a program for macromolecular energy, minimization and dynamics calculations. *J. Comput. Chem.* **4**, 187–217.

Bushweller, J. H., Billeter, M., Holmgren, A. & Wüthrich, K. (1994). The NMR solution structure of the mixed disulfide between *E. coli* glutaredoxin (14S) and glutathione. *J. Mol. Biol.* **235**, 1585–1597.

Cornell, W. D., Cieplak, P., Bayly, C. I., Gould, I. R., Merz, K. M., Jr, Ferguson, D. M., Spellmeyer, D. C., Fox, T., Caldwell, J. W. & Kollman, P. A. (1995). A second generation force filed for the simulation of protein, nucleic acids, and organic molecules. *J. Am. Chem. Soc.* **117**, 5179–5197.

Davis, D. A., Newcomb, F. M., Starke, D. W., Ott, D. E., Mieyal, J. J. & Yarchoan, R. (1997). Thioltransferase (glutaredoxin) is detected with HIV-1 and can regulate the activity of glutathionylated HIV-1 protease in vitro. *J. Biol. Chem.* **272**, 25935–25940.

Eklund, H., Ingelman, M., Söderberg, B.-O., Uhlin, T., Nordlund, P., Nikkola, M., Sonnerstam, U., Joelson, T. & Petratos, K. (1992). Structure of oxidized bacteriophage T4 glutaredoxin (thioredoxin). *J. Mol. Biol.* **228**, 596–618.

Farrow, N. A., Muhandiram, R., Singer, A. U., Pascal, S. M., Gish, G., Shoelson, S. E., Pawson, T., Forman-Kay, J. D. & Kay, L. E. (1994). Backbone dynamics of a free and phosphopeptide-complexed Src homology 2 domain studied by ^{15}N NMR relaxation. *Biochemistry,* **33**, 5984–6003.

Ferrin, T. E., Huang, C. C., Jarvis, L. E. & Langridge, R. (1988). The MIDAS display system. *J. Mol. Graph.* **6**, 13–27.

Forman-Kay, J. D., Clore, G. M. & Gronenborn, A. M. (1992). Relationship between electrostatics and redox function in human thioredoxin: characterization of pH titration shifts using two-dimensional homo- and heteronuclear NMR. *Biochemistry,* **31**, 3442–3452.

Gan, Z.-R. & Wells, W. W. (1987a). The primary structure of pig liver thioltransferase. *J. Biol. Chem.* **262**, 6699–6703.

Gan, Z.-R. & Wells, W. W. (1987b). Identification and reactivity of the catalytic site of pig liver thioltransferase. *J. Biol. Chem.* **262**, 6704–6797.

Gan, Z.-R., Polokoff, M. A., Jacobs, J. W. & Sordana, M. K. (1990). Complete amino acid sequence of yeast thioltransferase (glutaredoxin). *Biochem. Biophys. Res. Commun.* **168**, 944–951.

Gane, P. J., Freedman, R. B. & Warwicker, J. (1995). A molecular model for the redox potential difference between thioredoxin and DsbA, based on electrostatic calculations. *J. Mol. Biol.* **249**, 376–387.

Gladysheva, T. B., Oden, K. L. & Rosen, B. P. (1994). Properties of the arsenate reductase of plasmid R773. *Biochemistry,* **33**, 7288–729.

Gravina, S. A. & Mieyal, J. J. (1993). Thioltransferase is a specific glutathionyl mixed disulfide oxidoreductase. *Biochemistry,* **32**, 3368–3376.

Grzesiek, S., Kuboniwa, H., Hinck, A. P. & Bax, A. (1995). Multiple-quantum line narrowing for measurement of H^{α}-H^{β} *J* couplings in isotopically enriched proteins. *J. Am. Chem. Soc.* **117**, 5312–5315.

Güntert, P., Braun, W., Billeter, M. & Wüthrich, K. (1989). Automated stereospecific assignments and their impact on the precision of protein structure determinations in solution. *J. Am. Chem. Soc.* **111**, 3997–4004.

Güntert, P., Braun, W. & Wüthrich, K. (1991). Efficient computation of three-dimensional protein structures in solution from nuclear magnetic resonance data using the program DIANA and the supporting programs CALIBA, HABAS and GLOMSA. *J. Mol. Biol.* **217**, 517–530.

Güntert, P., Dötsch, V., Wider, G. & Wüthrich, K. (1992). Processing of multi-dimensional NMR data with the new software PROSA. *J. Biomol. NMR,* **2**, 619–629.

Güntert, P., Mumenthaler, C. & Wüthrich, K. (1997). Torsion angle dynamics for NMR structure calculation with the new program DYANA. *J. Mol. Biol.* **273**, 283–298.

Hol, W. G. (1985). The role of the alpha-helix dipole in protein function and structure. *Prog. Biophys. Mol. Biol.* **45**, 149–195.

Holmgren, A. (1976). Hydrogen donor system for *Escherichia coli* ribonuclease-diphosphate reductase dependent upon glutathione. *Proc. Natl Acad. Sci. USA,* **73**, 2275–2279.

Holmgren, A. (1979). Glutathione-dependent synthesis of deoxyribonucleotides. Purification and characterization of glutaredoxin from *Escherichia coli*. *J. Biol. Chem.* **254**, 3664–3671.

Höög, J.-O., Jörnvall, H., Holmgren, A., Carlquist, M. & Persson, M. (1983). The primary structure of *Escherichia coli* glutaredoxin. *Eur. J. Biochem.* **136**, 223–232.

Hopper, S., Johnson, R. S. & Biemann, K. (1989). Glutaredoxin from rabbit bone marrow. Purification, characterization and amino acid sequence determination by tandem mass spectrometry. *J. Biol. Chem.* **264**, 20438–20447.

Ingelman, M., Nordlund, P. & Eklund, H. (1995). The structure of a reduced mutant T4 glutaredoxin. *FEBS Letters,* **370**, 209–211.

Jeng, M. F., Campbell, A. P., Begley, T., Holmgren, A., Case, D. A., Wright, P. E. & Dyson, H. J. (1994). High-resolution solution structures of oxidized and reduced *Escherichia coli* thioredoxin. *Structure,* **2**, 853–868.

Jeng, M., Holmgren, A. & Dyson, H. J. (1995). Proton sharing between cysteine thiols in *Escherichia coli* thioredoxin: implication for the mechanism of protein disulfide reduction. *Biochemistry,* **34**, 10101–10105.

Johnson, G. P., Goebel, S. J., Perkus, M. E., Davies, S. W., Winslow, J. P. & Paoletti, E. (1991). Vaccinia virus encodes a protein with similarity to glutaredoxins. *Virology*, **181**, 378–381.

Jung, C. & Thomas, J. (1996). *S*-Glutathiolated hepatocyte proteins and insulin disulfides as substrates for reduction by glutaredoxin, thioredoxin, protein disulfide isomerase, and glutathione. *Arch. Biochem. Biophys.* **335**, 61–72.

Kallis, G. B. & Holmgren, A. (1980). Differential reactivity of the functional sulfhydryl groups of cysteine-32 and cysteine-35 present in the reduced form of thioredoxin from *Escherichia coli*. *J. Biol. Chem.* **255**, 10261–10265.

Karplus, M. & Petsko, G. A. (1990). Molecular dynamics simulation in biology. *Nature,* **347**, 631–639.

Katti, S. K., LeMaster, D. M. & Eklund, H. (1990). Crystal structure of thioredoxin from *Escherichia coli* at 1.68 Å resolution. *J. Mol. Biol.* **212**, 167–184.

Katti, S. K., Robbins, A. H., Yang, Y. & Wells, W. W. (1995). Crystal structure of thioltransferase at 2.2 Å resolution. *Protein Sci.* **4**, 1998–2005.

Kay, L. E., Keifer, P. & Saarinen, T. (1992). Pure absorption gradient enhanced heteronuclear single quantum correlation spectroscopy with improved sensitivity. *J. Am. Chem. Soc.* **114**, 10663–10665.

Kelley, J. J., III, Caputo, T. M., Eaton, S. F., Laue, T. M. & Bushweller, J. H. (1997). Comparison of backbone dynamics of reduced and oxidized *Escherichia coli* glutaredoxin-1 using 15N NMR relaxation measurements. *Biochemistry,* **36**, 5029–5044.

Klintrot, I.-M., Höög, J.-O., Jörnvall, H., Holmgren, A. & Luthman, M. (1984). The primary structure of calf thymus glutaredoxin. Homology with the corresponding *Escherichia coli* protein but elongation at both ends with an additional half-cysteine/cystine pair. *Eur. J. Biochem.* **144**, 417–423.

Koradi, R., Billeter, M. & Wüthrich, K. (1996). MOLMOL: a program for display and analysis of macromolecular structures. *J. Mol. Graph.* **14**, 51–55.

Kortemme, T. & Creighton, T. (1995). Ionisation of cysteine residues at the termini of model alpha-helical peptides. Relevance to unusual thiol pK_a values in proteins of the thioredoxin family. *J. Mol. Biol.* **253**, 799–821.

Kortemme, T., Darby, N. J. & Creighton, T. E. (1996). Electrostatic interactions in the active site of the N-terminal thioredoxin-like domain of protein disulfide isomerase. *Biochemistry,* **46**, 14503–14511.

Kren, B., Parsell, D. & Fuchs, J. A. (1988). Isolation and characterization of an *Escherichia coli* K-12 mutant deficient in glutaredoxin. *J. Bacteriol.* **170**, 308–315.

Kuboniwa, H., Grzesiek, S., Delaglio, F. & Bax, A. (1994). Measurement of H^N-H^α *J* couplings in calcium free calmodulin using new 2D and 3D water-flip-back methods. *J. Biomol. NMR,* **4**, 871–878.

Laskowski, R. A., Rullmann, J. A. C., MacArthur, M. W., Kaptein, R. & Thornton, J. M. (1996). AQUA and PROCHECK-NMR: programs for checking the quality of protein structures solved by NMR. *J. Biomol. NMR,* **8**, 477–486.

Luginbühl, P., Güntert, P., Billeter, M. & Wüthrich, K. (1996). The new program OPAL for molecular dynamics simulations and energy refinements of biological macromolecules. *J. Biomol. NMR,* **8**, 136–146.

Lundstrom-Ljung, J. & Holmgren, A. (1995). Glutaredoxin accelerates glutathione-dependent folding of reduced ribonuclease A together with protein disulfide-isomerase. *J. Biol. Chem.* **270**, 7822–7828.

Lundstrom-Ljung, J., Krause, G. & Holmgren, A. (1992). A Pro to His mutation in active site of thioredoxin increases its disulfide-isomerase activity 10-fold. *J. Biol. Chem.* **267**, 9047–9052.

Luthman, M. & Holmgren, A. (1982). Glutaredoxin from calf thymus. I. Purification to homogeneity. *J. Biol. Chem.* **257**, 6686–6690.

Luthman, M., Eriksson, S., Holmgren, A. & Thelander, L. (1979). Glutathione-dependent hydrogen donor system for calf thymus ribonucleoside diphosphate reductase. *Proc. Natl Acad. Sci. USA,* **76**, 2158–1262.

Martin, J. L., Bardwell, J. C. & Kuriyan, J. (1993). Crystal structure of the DsbA protein required for disulphide bond formation *in vivo*. *Nature,* **365**, 464–468.

Mieyal, J. J., Starke, D. W., Gravina, S. A. & Hocevar, B. A. (1991). Thioltransferase in human red blood cells: kinetics and equilibrium. *Biochemistry,* **30**, 8883–8891.

Minakuchi, K., Yabushita, T., Masumura, T., Ichihara, K. & Tanaka, K. (1994). Cloning and sequence analysis

of a cDNA encoding rice glutaredoxin. *FEBS Letters,* **337**, 157–160.

Muhandiram, D. R., Farrow, N. A., Xu, G., Smallcombe, S. H. & Kay, L. E. (1993). A gradient ^{13}C NOESY-HSQC experiment for recording NOESY spectra of ^{13}C-labeled proteins dissolved in H_2O. *J. Magn. Reson. ser. B,* **102**, 317–321.

Nelson, J. W. & Creighton, T. E. (1994). Reactivity and ionization of the active site cysteine residues of DsbA, a protein required for disulfide bond formation *in vivo*. *Biochemistry*, **33**, 5974–5983.

Padilla, C. A., Martínez-Galisteo, E., Bárcena, J. A., Spyrou, G. & Holmgren, A. (1995). Purification from placenta, amino acid sequence, structure comparisons and cDNA cloning of human glutaredoxin. *Eur. J. Biochem.* **227**, 27–34.

Padilla, C. A., Spyrou, G. & Holmgren, A. (1996). High-level expression of fully active human glutaredoxin (thioltransferase) in *E. coli* and characterization of Cys^7 to Ser mutant protein. *FEBS Letters,* **378**, 69–73.

Qin, J., Clore, G. M. & Gronenborn, A. M. (1994). The high-resolution three-dimensional solution structures of the oxidized and reduced states of human thioredoxin. *Structure,* **2**, 503–522.

Russel, M., Model, P. & Holmgren, A. (1990). Thioredoxin or glutaredoxin in *Escherichia coli* is essential for sulfate reduction but not for deoxyribonucleotide synthesis. *J. Bacteriol.* **172**, 1923–1929.

Sklenar, V., Torchia, D. A. & Bax, A. (1987). Measurement of carbon-13 longitudinal relaxation using ^1H detection. *J. Magn. Reson.* **73**, 375–379.

Sodano, P., Xia, T., Bushweller, J. H., Björnberg, O., Holmgren, A., Billeter, M. & Wüthrich, K. (1991). Sequence-specific ^1H N.M.R. assignments and determination of the three-dimensional structure of reduced *Escherichia coli* glutaredoxin. *J. Mol. Biol.* **221**, 1311–1324.

Sun, C., Holmgren, A. & Bushweller, J. H. (1997). Complete ^1H, ^{13}C, and ^{15}N NMR resonance assignments and secondary structure of human glutaredoxin in the fully reduced form. *Protein Sci*, **6**, 383–390.

Szyperski, T., Güntert, P., Otting, G. & Wüthrich, K. (1992). Determination of scalar coupling constants by inverse Fourier transformation of in-phase multiplets. *J. Magn. Reson.* **99**, 552–560.

Tsang, M. L. (1981). Assimilatory sulfate reduction in *Escherichia coli*: identification of the alternate cofactor for adenosine 3′-phosphate 5′-phosphosulfate reductase as glutaredoxin. *J. Bacteriol.* **146**, 1059–1066.

Weichsel, A., Gasdaska, J. R., Powis, G. & Montfort, W. R. (1996). Crystal structures of reduced, oxidized, and mutated human thioredoxins: evidence for a regulatory homodimer. *Structure,* **4**, 735–751.

Wells, W. W., Xu, D. P., Yang, Y. F. & Rocque, P. A. (1990). Mammalian thioltransferase (glutaredoxin) and protein disulfide isomerase have dehydroascorbate reductase activity. *J. Biol. Chem.* **265**, 15361–15364.

Wider, G. & Wüthrich, K. (1993). A simple experimental scheme using pulsed field gradients for coherence-pathway rejection and solvent suppression in phase-sensitive heteronuclear correlation spectra. *J. Magn. Reson. ser. B,* **102**, 239–241.

Xia, T. (1992). Software for Determination and Visual Display of NMR Structures of Proteins: the Distance Geometry Program DGPLAY and the Computer Graphics Programs CONFOR and XAM. PhD thesis no. 9831, ETH, Zürich, Switzerland.

Xia, T., Bushweller, J. H., Sodano, P., Billeter, M., Björnberg, O., Holmgren, A. & Wüthrich, K. (1992). NMR structure of oxidized *Escherichia coli* glutaredoxin: comparison with reduced *E. coli* glutaredoxin and functionally related proteins. *Protein Sci.* **10**, 310–321.

Yang, Y. & Wells, W. W. (1991). Identification and characterization of the functional amino acids at the active center of pig liver thioltransferase by site-directed mutagenesis. *J. Biol. Chem.* **266**, 12759–12765.

Zhang, O., Kay, L. E., Olivier, J. P. & Forman-Kay, J. D. (1994). Backbone ^1H and ^{15}N resonance assignments of the N-terminal SH_3 domain of dark in folded and unfolded states using enhanced-sensitivity pulsed field gradient NMR techniques. *J. Biomol. NMR,* **4**, 854–858.

Edited by P. E. Wright

(Received 24 February 1998; received in revised form 27 April 1998; accepted 29 April 1998)